Field strengths in oblique shock waves

Seiji Miyahara, Takahiro Kawashima, and Yukiharu Ohsawa
Department of Physics, Nagoya University, Nagoya 464-8602, Japan

(Received 6 August 2002; accepted 9 October 2002)

Large-amplitude oblique shock waves are studied with theory and particle simulations, with particular attention paid to electric and magnetic field strengths. First, by use of a two-fluid model, field strengths in a shock wave propagating obliquely to an external magnetic field are analytically obtained as functions of the Alfvén speed, shock speed, and propagation angle. Then, one-dimensional, relativistic, electromagnetic particle simulations are performed to test the theoretical prediction. The theory and simulation are found to be in good agreement for a wide range of angles. © *2003 American Institute of Physics.* [DOI: 10.1063/1.1526090]

I. INTRODUCTION

It has been long known that the Korteweg–de Vries (KdV) equation describes the evolution of small-amplitude magnetosonic waves; either perpendicular[1] or oblique waves.[2,3] Also, on the basis of a two-fluid model, exact solutions showing stationary perpendicular propagation of finite-amplitude pulses (or wave trains) have been found.[4–6] For a stationary, perpendicular solitary pulse, the maximum value of the magnetic field, B_m, is related to the Alfvén Mach number M through

$$B_m/B_0 = 2M - 1, \tag{1}$$

where B_0 is the magnetic field strength in the far upstream region. This theory is valid for $1 < M < 2$. Later, this theory was improved so that we can deal with a relativistic regime where the electron fluid velocity is comparable to the speed of light c;[7] the electron velocity parallel to the wave front is especially high in a perpendicular magnetosonic wave. We have the same relation (1) in this case, and M is also in the region $1 < M < 2$.

On the other hand, particle simulations have shown that a magnetosonic shock wave can accelerate particles with nonstochastic mechanisms.[8–20] These studies prompted us to investigate large-amplitude magnetosonic waves; the study of particle acceleration requires the knowledge of the structure of nonlinear magnetosonic waves. Nakazawa and Ohsawa[21,22] then discussed the field strengths in perpendicular shock waves with $M \gtrsim 2$ and obtained the magnetic field strength as

$$B_m/B_0 = 1 + \gamma_{\rm sh}^2[(1+2M^2)^{1/2} - 1], \tag{2}$$

where $\gamma_{\rm sh}$ is the Lorentz factor for the shock propagation speed $v_{\rm sh}$.

We would also like to know field strengths in oblique shock waves. We would then be able to theoretically estimate particle energies accelerated in these waves. For instance, the maximum energy of ultrarelativistic electrons is expressed in terms of the maximum value of the electric potential.[19,20] The magnitude of energy jump of incessantly accelerated fast ions is proportional to the transverse electric field.[17,18]

In this paper, we extend the above theory[21,22] to oblique shock waves and discuss the field strengths in the waves. In Sec. II, we analytically obtain the maximum values of electromagnetic fields and electric potential in large-amplitude, oblique shock waves with $M \gtrsim 2$. In Sec. III, we carry out one-dimensional, relativistic, electromagnetic, particle simulations and measure the field strengths of shock waves. We make comparisons with theoretically obtained field strengths and simulation results. It is found that the theory and simulation are in good agreement for a wide range of propagation angles. In Sec. IV, we summarize our work.

II. ESTIMATE OF FIELD STRENGTHS

We consider a shock wave propagating in the x direction with a propagation speed $v_{\rm sh}$ in an external magnetic field that is in the (x,z) plane (see Fig. 1):

$$\boldsymbol{B}_{l0} = B_{l0}(\cos\theta, 0, \sin\theta), \tag{3}$$

where the subscript l refers to the quantities in the laboratory frame, and the subscript 0 indicates the far upstream region. The wave is assumed to be stationary. In the wave frame, therefore, the time derivatives in the fluid equations are zero, $\partial/\partial t = 0$. Accordingly, the y component of the electric field is constant,

$$E_{wy} = E_{wy0} = -(v_{\rm sh}/c)B_{wz0}, \tag{4}$$

where the subscript w denotes the wave frame. The z component is zero; $E_{wz} = 0$. For one-dimensional propagation with $\partial/\partial y = \partial/\partial z = 0$, the x component of the magnetic field is constant,

$$B_{wx} = B_{wx0} = B_{lx0}. \tag{5}$$

In the upstream region, we have the relation

$$B_{wz0} = \gamma_{\rm sh} B_{lz0}, \tag{6}$$

where $\gamma_{\rm sh} = (1 - v_{\rm sh}^2/c^2)^{-1/2}$. The upstream plasma velocity has a component parallel to the magnetic field given as

$$v_{w\parallel 0} = -v_{\rm sh} B_{wx0}/B_{w0}. \tag{7}$$

We discuss the field strengths of the shock wave on the basis of the two-fluid model:

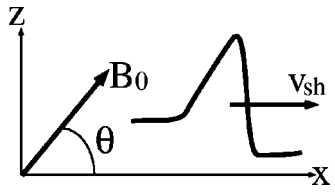

FIG. 1. Geometery of shock wave and magnetic field.

$$\frac{\partial n_j}{\partial t}+\nabla\cdot(n_j\boldsymbol{v}_j)=0, \tag{8}$$

$$m_j\left(\frac{\partial}{\partial t}+(\boldsymbol{v}_j\cdot\nabla)\right)(\gamma_j\boldsymbol{v}_j)=q_j\boldsymbol{E}+\frac{q_j}{c}\boldsymbol{v}_j\times\boldsymbol{B}, \tag{9}$$

$$\frac{1}{c}\frac{\partial\boldsymbol{B}}{\partial t}=-\nabla\times\boldsymbol{E}, \tag{10}$$

$$\frac{1}{c}\frac{\partial\boldsymbol{E}}{\partial t}=\nabla\times\boldsymbol{B}-\frac{4\pi}{c}\sum_j n_jq_j\boldsymbol{v}_j, \tag{11}$$

where the subscript j refers to ions ($j=i$) or electrons ($j=e$); m_j is the mass, q_j is the charge, n_j is the number density, and $\boldsymbol{v}_j$ is the velocity.

We assume that B_z and electric potential ϕ have their maximum values at the same point, $x=x_m$, and that the y component of the magnetic field is nearly zero there. In small-amplitude magnetosonic waves, this is mathematically proved.[2,3] We suppose that this is also valid for large-amplitude waves; simulation results are consistent with this assumption.[19,20]

A. Maximum value of B_{wz}

Since the time derivatives are zero in the wave frame, the continuity equation, (8), gives

$$n_{wj}v_{wjx}=-n_{wj0}v_{\mathrm{sh}}. \tag{12}$$

We multiply the x component of Eq. (9) by n_{wj} and sum over particle species to have

$$\sum_j m_jn_{wj}v_{wjx}\frac{d(\gamma_{wj}v_{wjx})}{dx}=\sum_j q_jn_{wj}\left(E_{wx}+\frac{v_{wjy}}{c}B_{wz}-\frac{v_{wjz}}{c}B_{wy}\right). \tag{13}$$

Combining Eqs. (11), (12), (13), and Gauss' law, we find that

$$\frac{d}{dx}\left(-\sum_j m_jn_{w0}v_{\mathrm{sh}}\gamma_{wj}v_{wjx}+\frac{B_{wy}^2+B_{wz}^2-E_{wx}^2}{8\pi}\right)=0, \tag{14}$$

which is integrated to give

$$\frac{B_{wy}^2+B_{wz}^2-B_{wz0}^2-E_{wx}^2}{8\pi}=\sum_j m_jn_{w0}v_{\mathrm{sh}}(\gamma_{\mathrm{sh}}v_{\mathrm{sh}}+\gamma_{wj}v_{wjx}). \tag{15}$$

Around the point x_{wm}, both B_{wy} and E_{wx} are small. Furthermore, v_{wjx} must be small in magnitude compared with the far upstream speed v_{sh}, because the plasma density is high at $x_w=x_{wm}$. (We are concerned with large-amplitude waves.) We therefore obtain the maximum value of B_{wz} as

$$\frac{B_{wzm}}{B_{wz0}}=\left(1+\frac{m_in_{w0}\gamma_{\mathrm{sh}}v_{\mathrm{sh}}^2}{B_{wz0}^2/(8\pi)}\right)^{1/2}, \tag{16}$$

where the electron term has been neglected.

B. Maximum value of ϕ_w

If we neglect the electron inertia in the momentum equation, (9), we may express the electron fluid velocity as

$$v_{wex}=\frac{cE_{wy0}B_{wz}}{B_w^2}+\frac{v_{we\parallel}B_{wx0}}{B_w}, \tag{17}$$

$$v_{wey}=-\frac{cE_{wx}B_{wz}}{B_w^2}+\frac{v_{we\parallel}B_{wy}}{B_w}, \tag{18}$$

$$v_{wez}=\frac{c(E_{wx}B_{wy}-E_{wy0}B_{wx0})}{B_w^2}+\frac{v_{we\parallel}B_{wz}}{B_w}, \tag{19}$$

where $v_{we\parallel}$ is the electron fluid velocity parallel to the magnetic field. Substituting Eq. (18) in the y component of Eq. (11) yields

$$\frac{dB_{wz}}{dx}=-\frac{4\pi n_{wi}ev_{wiy}}{c}+\frac{4\pi n_{we}e}{c}\times\left(-\frac{cE_{wx}B_{wz}}{B_w^2}+\frac{v_{we\parallel}B_{wy}}{B_w}\right). \tag{20}$$

We eliminate the electron density n_{we} using Eq. (12). By virtue of Eqs. (4) and (17), we then have the longitudinal electric field ($E_{wx}=-\partial\phi_w/\partial x$) as

$$\frac{\partial\phi_w}{\partial x}=\left(B_{wz0}-\frac{v_{we\parallel}}{v_{\mathrm{sh}}}\frac{B_{wx0}B_w}{B_{wz}}\right)\left(\frac{1}{4\pi n_{we0}e}\frac{dB_{wz}}{dx}+\frac{n_{wi}v_{wiy}}{n_{we0}c}\right)-\frac{v_{we\parallel}}{c}\frac{B_{wy}B_w}{B_{wz}}. \tag{21}$$

The first and second terms in the first parentheses on the right-hand side of Eq. (21) arise from the $\boldsymbol{E}\times\boldsymbol{B}$ drift and parallel velocity terms in Eq. (17), respectively.

Because the shock width is of the order of c/ω_{pi}, where ω_{pi} is the ion plasma frequency, the ratio of the second term to the first one in the second parentheses on the right-hand side of Eq. (21) is estimated to be $\sim B_{wx0}B_{wy}/[B_{w0}(B_{wzm}-B_{wz0})]$, which will be much smaller than unity if $B_{wz0}\gtrsim B_{wx0}$ (see the Appendix). The second term is thus neglected. Also, we neglect the last term, because B_{wy} is small compared with the other magnetic field components; B_{wy} is zero in the upstream region and at $x_w=x_{wm}$, while B_{wz} is greatly enhanced in the shock region.

Neglecting the change in $v_{we\parallel}$, we substitute Eq. (7) for electrons in Eq. (21) and integrate it from $x=\infty$ to $x=x_m$. We may then express the maximum value of the potential as

$$\phi_{wm}=\phi_{wmd}+\phi_{wm\parallel}, \tag{22}$$

where ϕ_{wmd} indicates the potential related to the $\boldsymbol{E}\times\boldsymbol{B}$ drift [the first term in the first parentheses on the right-hand side

of (21)], while $\phi_{wm\parallel}$ is due to the electron motion parallel to the magnetic field (the second term in the same parentheses). They are given as

$$\phi_{wmd}=\frac{B_{wz0}(B_{wzm}-B_{wz0})}{4\pi n_{we0}e}, \tag{23}$$

$$\phi_{wm\parallel}=\frac{B_{wx0}^2}{4\pi n_{we0}eB_{w0}}\int_{\infty}^{x_m}\frac{B_w}{B_{wz}}\frac{dB_{wz}}{dx}dx. \tag{24}$$

We then show that, for propagation angles such that $B_{wx0}^2/B_{wz0}^2<1$, ϕ_{wmd} is larger than $\phi_{wm\parallel}$. Moreover, ϕ_{wmd} would predominate over $\phi_{wm\parallel}$ in large-amplitude waves even for $B_{wz0}/B_{wx0}\sim 1$. For small amplitude waves, B_w/B_{wz} in Eq. (24) can be approximated as B_{w0}/B_{wz0}, and Eq. (24) is integrated as

$$\phi_{wm\parallel}=\frac{B_{wx0}^2(B_{wzm}-B_{wz0})}{4\pi n_{we0}eB_{wz0}}. \tag{25}$$

On the other hand, the z component of the magnetic field is greatly increased in the shock region. Therefore, if the angle is not so small, i.e., if $B_{wz0}/B_{wx0}\gtrsim 1$, large-amplitude waves would have the relation $B_w/B_{wz}\sim 1$ in the shock region. Then, Eq. (24) gives

$$\phi_{wm\parallel}=\frac{B_{wx0}^2(B_{wzm}-B_{wz0})}{4\pi n_{we0}eB_{w0}}. \tag{26}$$

The ratio of Eq. (25) to Eq. (23) is B_{wx0}^2/B_{wz0}^2, while the ratio of (26) to (23) is $B_{wx0}^2/(B_{w0}B_{wz0})$. The latter is thus B_{wz0}/B_{w0} times as small as the former. Hence, we see that ϕ_{wmd} is much larger than $\phi_{wm\parallel}$ in both small- and large-amplitude waves, when $B_{wx0}^2/B_{wz0}^2\ll 1$. Furthermore, $\phi_{wm\parallel}$ becomes less important than ϕ_{wmd} as the wave-amplitude increases.

C. Maximum field values in the laboratory frame

We now obtain the field strengths in the laboratory frame. From Eqs. (4), (6), and the relation

$$B_{lz}=\gamma_{\rm sh}[B_{wz}+(v_{\rm sh}/c)E_{wy0}], \tag{27}$$

it follows that

$$\frac{B_{lzm}}{B_{lz0}}=1+\gamma_{\rm sh}^2\left(\frac{B_{wzm}}{B_{wz0}}-1\right). \tag{28}$$

Substituting Eq. (16) in Eq. (28) and then using the relations $n_{w0}=\gamma_{\rm sh}n_{l0}$ and $B_{wz0}=\gamma_{\rm sh}B_{lz0}$, we find the maximum value of B_z in the laboratory frame as

$$\frac{B_{lzm}}{B_{lz0}}=1+\gamma_{\rm sh}^2\left[\left(1+\frac{2v_{\rm sh}^2}{v_{\rm A}^2\sin^2\theta}\right)^{1/2}-1\right], \tag{29}$$

where $v_{\rm A}$ is the Alfvén speed defined in the laboratory frame,

$$v_{\rm A}=B_{l0}/(4\pi n_{l0}m_i)^{1/2}, \tag{30}$$

and θ is the angle introduced by Eq. (3); i.e., $\tan\theta=B_{lz0}/B_{lx0}$.

In the laboratory frame, the maximum value of the transverse electric field E_y is related to the magnetic field through

$$E_{lym}=(v_{\rm sh}/c)(B_{lzm}-B_{lz0}). \tag{31}$$

Substitution of Eq. (29) in (31) gives

$$\frac{E_{lym}}{B_{lz0}}=\frac{\gamma_{\rm sh}^2v_{\rm sh}}{c}\left[\left(1+\frac{2v_{\rm sh}^2}{v_{\rm A}^2\sin^2\theta}\right)^{1/2}-1\right]. \tag{32}$$

The potential in the Lorentz gauge in the laboratory frame, $\phi_{l\rm L}$, may be given as

$$\phi_{l\rm L}=\gamma_{\rm sh}\phi_w, \tag{33}$$

since the x component of the vector potential in the wave frame can be taken to be zero; $A_{wx}=0$. For a stationary wave propagating with the speed $v_{\rm sh}$, the potential in the Coulomb gage is thus given as[22]

$$\phi_{l\rm C}=\phi_w/\gamma_{\rm sh}. \tag{34}$$

With the aid of Eqs. (16), (23), (26), and (34), we obtain the maximum value of the potential as

$$e\phi_{l{\rm C}m}=m_iv_{\rm A}^2\left(\sin^2\theta+\frac{\sin\theta\cos\theta}{\gamma_{\rm sh}(1+\gamma_{\rm sh}^2\tan^2\theta)^{1/2}}\right)\times\left[\left(1+\frac{2v_{\rm sh}^2}{v_{\rm A}^2\sin^2\theta}\right)^{1/2}-1\right]. \tag{35}$$

The term proportional to $1/(1+\gamma_{\rm sh}^2\tan^2\theta)^{1/2}$ in Eq. (35) arises from $\phi_{we\parallel}$, Eq. (26). [Here, we did not use Eq. (25), but used Eq. (26), because we are interested in large-amplitude waves.] The other part is due to ϕ_{wmd},

$$e\phi_{l{\rm C}md}=m_iv_{\rm A}^2\sin^2\theta\left[\left(1+\frac{2v_{\rm sh}^2}{v_{\rm A}^2\sin^2\theta}\right)^{1/2}-1\right]. \tag{36}$$

This is the main part of the potential for $\theta\gtrsim 45°$.

In the limit of $\theta=90°$, Eqs. (29), (32), and (35) reduce to the ones obtained for perpendicular waves; Eqs. (17) and (20) in Ref. 21 and Eq. (1) in Ref. 22, respectively.

The obtained field strengths are valid when the propagation angles are not small. We here summarize the reasons for this. First, we have explicitly used this assumption in the above calculations. For instance, if B_{wz0} is much smaller than B_{wx0}, then the value of (A4) may be of the order of unity; accordingly, the term proportional to v_{wiy} in Eq. (21) cannot be neglected. Also, in deriving $\phi_{wm\parallel}$, Eq. (26), we assumed that $B_{wz0}/B_{wx0}\gtrsim 1$. Second, the density perturbation n_1 in the magnetosonic wave becomes small compared with the magnetic perturbation B_{z1} as the propagation angle θ decreases; for small-amplitude waves, we have a relation $n_1/n_0\simeq\sin\theta(B_{z1}/B_0)$.[2,3] If the density perturbation is small, then v_{wjx} at $x=x_{wm}$ will not be sufficiently small. Hence, it will not be a good approximation to neglect the term $\gamma_{wj}v_{wjx}$ compared with $\gamma_{\rm sh}v_{\rm sh}$ in Eq. (15). Third, for small propagation angles, the dispersion effect would violate the assumption of stationary propagation. When θ is small, short-wavelength perturbations can propagate faster than the shock wave, going away ahead of the shock wave; thus, the region in front of the main pulse will not be stationary.

III. COMPARISON OF THEORY AND PARTICLE SIMULATION

We now test the theory developed in Sec. II, by using a one-dimensional, relativistic, electromagnetic, particle simu-

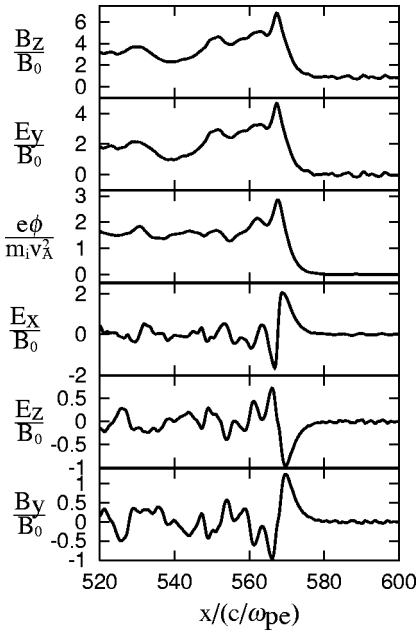

FIG. 2. Snapshots of field profiles of an oblique shock wave with $\theta=60°$.

lation code with full ion and electron dynamics.[23] In the simulations, we observe self-consistent evolution of shock waves and measure the field strengths in the waves. The details of the simulation method can be found in Refs. 11, 19, and 23. The simulation parameters are as follows: The numbers of simulation particles are $N_i=N_e=262$, 144, and the grid size is $L_x=4096\Delta_g$, where Δ_g is the grid spacing. The ion-to-electron mass ratio is $m_i/m_e=100$. The ratio of the electron cyclotron frequency ω_{ce} to the electron plasma frequency ω_{pe} is $\omega_{ce}/\omega_{pe}=3.0$ in the upstream region. The light speed is $c=4.0$, where the velocity is normalized to $\omega_{pe}\Delta_g$. The Alfvén speed is $v_A=1.2$. The electron and ion thermal velocities are v_{Te} $[=(T_e/m_e)^{1/2}]=0.46$ and v_{Ti} $=0.046$, respectively. Because all the simulation results are shown in the laboratory frame, we omit the subscript l in this section.

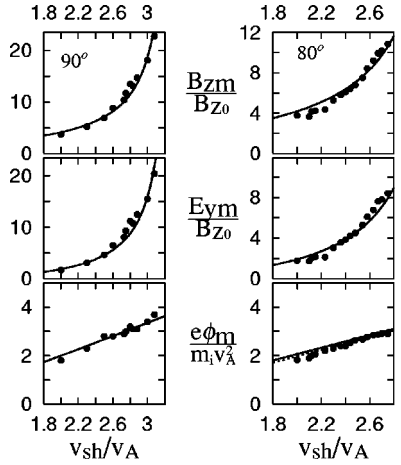

FIG. 3. Field strength versus Alfvén Mach number for $\theta=90°$ and for $\theta=80°$. Theory (solid lines) and simulations (dots) for B_z, E_y, and ϕ are shown.

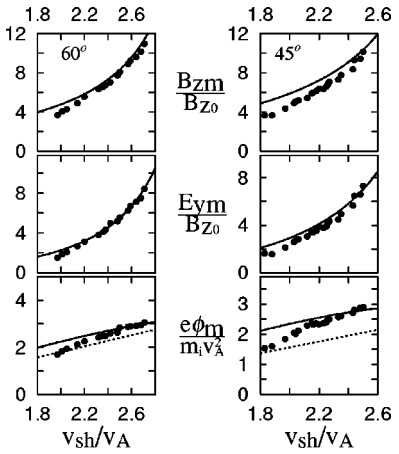

FIG. 4. Field strength versus Alfvén Mach number for $\theta=60°$ and for $\theta=45°$. The dotted lines show ϕ_{md}.

As an example of oblique shock waves observed in the simulations, we show in Fig. 2 snapshots of field profiles of a shock wave with a propagation angle $\theta=60°$ and propagation speed $v_{sh}=2.5v_A$. The fields B_z, E_y, and ϕ take their maximum values at nearly the same x position, while E_x, E_z, and B_y have values close to zero around this position. This is consistent with the assumption made in the theory.

Carrying out these simulations, we have measured field strengths of various shock waves. We show in Fig. 3 the maximum values of B_z, E_y, and ϕ of shock waves with a propagation angle $\theta=90°$ (left panels) and with $\theta=80°$ (right panels) as functions of the Alfvén Mach number, $M=v_{sh}/v_A$. The solid lines represent the theory; Eqs. (29), (32), and (35). The dots show simulation results. We show in Fig. 4 the same quantities for propagation angle $\theta=60°$ (left panels) and for $\theta=45°$ (right panels). The dashed lines in the panels for ϕ indicate the magnitude of ϕ_{md}; potential (36) that is related to the $\boldsymbol{E}\times\boldsymbol{B}$ drift. These figures show that the theory and simulation are in good agreement. The simulation, however, tends to give slightly smaller values than the theoretical ones for small angles and low Mach numbers. For the potential at $\theta=45°$, the simulation values for $M\simeq 2$ are about 80% of the theoretical values. It is also noted that ϕ_{md} is about 80% of the total potential ϕ_m in the theoretical calculations for $\theta=60°$. Its ratio increases with increasing angle θ; at $\theta=90°$, ϕ_{md} is equal to the total potential ϕ_m.

We briefly mention the waves with small θ. We show in Fig. 5 a snapshot of B_z for a shock wave with $\theta=30°$ and $v_{sh}/v_A=2.1$. This wave profile is quite different from those in Fig. 2. In front of the main pulse, wave trains are propagating faster than the shock wave, owing to the positive

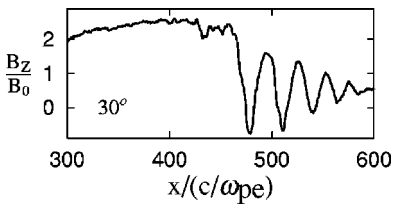

FIG. 5. Profile of B_z for $\theta=30°$.

dispersion.[2,3] We do not observe a high peak near the shock front. For such shock waves, the maximum value of B_z is much smaller than the theoretical one. In our simulations for $\theta=30°$, which are not shown here, observed values of ϕ_m with $M\sim 2$ were only $\sim 30\%$ of those given by (35). [As is evident from the derivation, Eq. (35) is not supposed to be applicable to such waves.] The region of angles for which the wave trains become significant may depend on plasma parameters such as the strength of the external magnetic field and plasma density.

IV. SUMMARY

We have studied the field strengths in oblique shock waves. On the basis of the two-fluid model, we theoretically obtained the maximum values of B_z, E_y, and ϕ as functions of the Alfvén speed v_A, shock speed v_{sh}, and propagation angle θ, assuming that the amplitude is large and that the propagation angle is large, $\theta \gtrsim 45°$. We then performed particle simulations of perpendicular and oblique shock waves and measured field strengths in the waves. The theoretically obtained field values for large-amplitude waves, $M \gtrsim 2$, were in good agreement with the simulation results for a wide range of propagation angles.

ACKNOWLEDGMENTS

This work was carried out by the joint research program of the Solar–Terrestrial Environment Laboratory, Nagoya University, and was supported in part by a Grant-in-Aid for Scientific Research from the Japan Society for the Promotion of Science.

APPENDIX: ION VELOCITY PARALLEL TO THE WAVE FRONT

The ion velocity in the y direction is much smaller than the Alfvén speed. We here estimate its magnitude. From the y component of the equation of motion (9), we have

$$v_{wx}\frac{d(\Sigma_j m_j \gamma_{wj} v_{wjy})}{dx}=e\frac{(v_{wiz}-v_{wez})}{c}B_{wx0}, \tag{A1}$$

where we have used the relation

$$v_{wix}\simeq v_{wex}=v_{wx}, \tag{A2}$$

which approximately holds in magnetohydrodynamic waves because of the charge neutrality. For angles very close to $\theta=90°$, v_{wey} is much larger than v_{wiy} in magnitude.[4,5,7] In oblique waves, however, v_{wey} and v_{wiy} are of the same order of magnitude.[2,3] We therefore neglect the term of electron momentum in (A1). On account of the z component of Eq. (11) and Eq. (12), we find that

$$v_{wiy}=\frac{B_{wx0}B_{wy}}{4\pi m_i n_{w0} v_{sh}\gamma_{wi}}. \tag{A3}$$

This indicates that $v_{wiy}/v_{wA}=(v_{wA}/v_{sh})B_{wx0}B_{wy}/B_{w0}^2$, where v_{wA} is the Alfvén speed in the wave frame. We thus have

$$\left(\frac{n_{wi}v_{wiy}}{n_{we0}c}\right)\Big/\left(\frac{1}{4\pi n_{we0}e}\frac{dB_{wz}}{dx}\right) \sim \frac{n_{wi}v_{wA}B_{wx0}B_{wy}}{n_{wi0}v_{sh}B_{w0}(B_{wzm}-B_{wz0})}. \tag{A4}$$

Because B_{wy} is small compared with the other magnetic field components, this is small for large-amplitude waves if $B_{wz0} \gtrsim B_{wx0}$.

In the same way, by virtue of the z component of Eq. (9) and the y component of Eq. (11), we obtain

$$v_{wiz}(x_m)=\frac{B_{wx0}(B_{wzm}-B_{wz0})}{4\pi m_i n_{w0} v_{sh}\gamma_{wi}}. \tag{A5}$$

[1] C. S. Gardner and G. K. Morikawa, Commun. Pure Appl. Math. **18**, 35 (1965).
[2] T. Kakutani, H. Ono, T. Taniuti, and C. C. Wei, J. Phys. Soc. Jpn. **24**, 1159 (1968).
[3] Y. Ohsawa, Phys. Fluids **29**, 1844 (1986).
[4] J. H. Adlam and J. E. Allen, Philos. Mag., Suppl. **3**, 448 (1958).
[5] L. Davis, R. Lüst, and A. Schlüter, Z. Naturforsch. Teil A **13**, 916 (1958).
[6] R. Z. Sagdeev, in *Reviews of Plasma Physics*, edited by M. A. Leontovich (Consultants Bureau, New York, 1966), Vol. 4, pp. 23–91.
[7] Y. Ohsawa, Phys. Fluids **29**, 2474 (1986).
[8] D. Biskamp and H. Welter, Nucl. Fusion **12**, 663 (1972).
[9] M. M. Leroy, D. K. Winske, C. C. Goodrich, C. S. Wu, and K. Papadopoulos, J. Geophys. Res., [Oceans] **87**, 5081 (1982).
[10] D. W. Forslund, K. B. Quest, J. U. Brackbill, and K. Lee, J. Geophys. Res., [Oceans] **89**, 2142 (1984).
[11] Y. Ohsawa, Phys. Fluids **28**, 2130 (1985).
[12] Y. Ohsawa, J. Phys. Soc. Jpn. **55**, 1047 (1986).
[13] R. L. Tokar, S. P. Gary, and K. B. Quest, Phys. Fluids **30**, 2569 (1987).
[14] B. Lembege and J. M. Dawson, Phys. Fluids B **1**, 1001 (1989).
[15] M. Toida and Y. Ohsawa, Sol. Phys. **171**, 161 (1997).
[16] K. Maruyama, N. Bessho, and Y. Ohsawa, Phys. Plasmas **5**, 3257 (1998).
[17] S. Usami, H. Hasegawa, and Y. Ohsawa, Phys. Plasmas **8**, 2666 (2001).
[18] S. Usami and Y. Ohsawa, Phys. Plasmas **9**, 1069 (2002).
[19] N. Bessho and Y. Ohsawa, Phys. Plasmas **6**, 3076 (1999).
[20] N. Bessho and Y. Ohsawa, Phys. Plasmas **9**, 979 (2002).
[21] S. Nakazawa and Y. Ohsawa, J. Phys. Soc. Jpn. **66**, 2044 (1997).
[22] S. Nakazawa and Y. Ohsawa, J. Phys. Soc. Jpn. **66**, 2965 (1997).
[23] P. C. Liewer, A. T. Lin, J. M. Dawson, and M. Z. Caponi, Phys. Fluids **24**, 1364 (1981).